

# Flexible Nanowire Cathode Membrane with Gradient Interfaces and Rapid Electron/Ion Transport Channels for Solid-State Lithium Batteries

Yu Cheng, Jun Shu, Lin Xu,\* Yangyang Xia, Lulu Du, Gang Zhang, and Liqiang Mai\*

Solid-state lithium batteries (SSLBs) have attracted more attention due to their improved safety and high energy density. Although numerous solid-state electrolytes (SSEs) with high ionic conductivity have been frequently reported, poor solid–solid interfacial contact and interfacial chemical reactions around the cathode in SSLBs can hinder their practical application. Here, a gradient nanowire (NW) cathode is demonstrated for advanced interface engineering in SSLBs by a facile solvent evaporation process. In this unique gradient cathode membrane, one side surface with more ionic conductive polymer provides a smooth contact with SSE, while the other side surface with more electronic conductive NW/reduced graphene oxide composite provides rapid electron transport acting as a current collector. Furthermore, the inside NW cathode materials are uniformly coated by a solid polymer electrolyte and such a structure changes the point-to-point contact to a large-area contact in the cathode, providing continuous channels for rapid electron/ion transport and improved mechanical strength. The effective interface engineering gives SSLBs enhanced structural stability and excellent electrochemical performance. The as-obtained SSLBs can deliver 200 mAh g<sup>-1</sup> capacity after 100 cycles at room temperature without obvious structural degradation. This novel design of NW-based gradient cathodes demonstrates a promising strategy for solid–solid interface engineering in solid-state lithium batteries.

conductivity and interface issues in SSLBs are still two main difficulties to be overcome. Although high ionic conductivity of solid-state electrolytes (SSEs) has been achieved, the solid–solid interface issues severely impede the development of practical application in SSLBs, especially about interfaces in cathode materials.<sup>[4,5]</sup> In terms of the cathode/SSE interface, one main issue is poor physical contact.<sup>[6,7]</sup> It results in increased interface impedance and inefficient lithium-ion transport. After several cycles, volume expansion/contraction of cathode materials will lead to physical delamination.<sup>[8,9]</sup> Another problem is the intrinsic electrochemical instability between the cathode/SSE interface, especially in SSLBs with sulfide solid electrolytes.<sup>[10]</sup> As a result, complex side reactions significantly reduce the interface compatibility, and the by-products formed after electrolyte degradation will greatly increase the impedance of batteries.<sup>[11,12]</sup> Apart from the cathode/SSE interface, the internal interface in the bulk cathode material is another bottleneck.<sup>[13]</sup> The gaps between particles in the bulk cathode of SSLBs fail to be connected as in the liquid

electrolyte. Furthermore, the strength of point-to-point interfacial contact will also be more fragile under the volume change during cycling.<sup>[14]</sup>

To achieve beneficial compatibility between the electrode/SSE interface, artificial buffer layers were applied to optimize the interfaces in SSLBs.<sup>[15,16]</sup> They can provide steady interfaces with enhanced physical contacts and chemical/electrochemical stabilities. During the past several years, considerable related researches about coating-modified electrode/SSE interfaces have been reported, and great success has been achieved.<sup>[17,18]</sup> Although these methods can mitigate the interfacial problems to some extent, point-to-point contact between inside cathode particles is still remained to be solved. To overcome this phenomenon, buffer layers coating on individual cathode particles have been successively reported.<sup>[14,19]</sup> This core–shell structure makes use of the large contact area and numerous channels for rapid Li<sup>+</sup> transport, thus cathodes with higher Li<sup>+</sup> transport efficiency and lower interfacial impedance were fabricated. However, the sharp interfaces between SSE/bulk cathode and cathode/current collector still remain to be solved. The


## 1. Introduction

Solid-state lithium batteries (SSLBs) have been widely concerned and valued in recent years because of increased safety and high energy density.<sup>[1–3]</sup> However, problems like ionic

Dr. Y. Cheng, J. Shu, Prof. L. Xu, Y. Y. Xia, Dr. L. L. Du, G. Zhang, Prof. L. Q. Mai  
State Key Laboratory of Advanced Technology for Materials Synthesis  
and Processing

School of Materials Science and Engineering  
Wuhan University of Technology  
Wuhan, Hubei 430070, P. R. China  
E-mail: linxu@whut.edu.cn; mlq518@whut.edu.cn

Prof. L. Xu, Prof. L. Q. Mai  
Foshan Xianhu Laboratory of the Advanced Energy Science  
and Technology Guangdong Laboratory  
Xianhu Hydrogen Valley  
Foshan 528200, P. R. China

 The ORCID identification number(s) for the author(s) of this article can be found under <https://doi.org/10.1002/aenm.202100026>.

DOI: 10.1002/aenm.202100026

point-to-point contact and uncovered gaps between particles formed by bonding or simple stacking still cannot be fully infiltrated by SSE as same as the liquid electrolyte. And the coating thickness of SSE also affects the electron transport in the system.<sup>[20]</sup> In addition, the cracks of some inorganic buffer layer were observed after cycling due to the volume change of cathode particles, which significantly decreased the cycling stability of SSLBs.<sup>[21,22]</sup> Solid polymer electrolyte (SPE) is one of the promising SSEs due to the soft contact with electrode and outstanding interface compatibility.<sup>[23,24]</sup> Chen et al. fabricated a cathode-supported SSE framework by a brief tape-casting approach, polymer filled the gaps between cathode materials.<sup>[20]</sup> The as-obtained integrated SSLBs possessed better electrochemical performance than SSLBs with the conventional cathode, indicating the significant enhancement of interfacial contact between SPE and cathode. Moreover, SPE as a buffer layer successfully endures the volume change of cathode materials during cycling owing to the flexibility and tight attachment.<sup>[25,26]</sup> However, it still remains an issue to be solved that the pores in the tape casting cathode (noted as homogeneous cathode) are formed by simple random stacking of particles, which are disordered and hard to be controlled, even though the polymer melts and penetrates the pores, uniform and effective coating on every single particle is difficult to be achieved.

Therefore, constructing benign interfacial contact and arranged electron/ion transport channels between electrode/SSE are great challenges. The flexibility of nanowire (NW) materials can effectively relieve the interfacial pressure caused by volume expansion during cycling as electrode materials, and provide direct pathways for rapid ionic conduction as additives in solid polymer materials.<sup>[27–29]</sup> As for cathode materials, vanadium oxide materials have been noted as promising electrode materials for various battery systems because of their high theoretical capacity,<sup>[30]</sup> which have also been used as cathode materials in SSLBs.<sup>[31,32]</sup> Herein, we demonstrate a gradient NW cathode for advanced interface engineering in SSLBs. In this unique gradient cathode, two polyethylene oxide (PEO) gradient distribution interfaces are constructed as interface buffer layers at two surfaces. One side surface with more ionic conductive polymer provides smooth contact with SSE, while the other side surface with more electronic conductive  $\text{H}_2\text{V}_3\text{O}_8$  NWs/rGO (reduced graphene oxide) provides rapid electron transport as current collector. Furthermore, the inside NW cathode materials are uniformly coated by rGO and PEO-based SPE as the main cathode body, and such strong combination changes the point-to-point contact to large-area contact between cathode/SSE, providing continuous channels for rapid electron/ion transport and improved structural stability. All the interspaces in the bulk cathode are filled by SPE, reinforcing the structural strength of the integrated cathode. Owing to the interface engineering of cathode/SSE, cathode/current collector, and the inner structure in the cathode, the SSLBs with this novel gradient NW cathode membrane possess higher lithium-ion diffusion efficiency, lower impedance, excellent cycling capacity, and stability. Hence, this new design of gradient interface engineering opens a new avenue for solving the challenges of solid–solid interface problems in SSLBs.

## 2. Results and Discussion

In the traditional preparation method of cathode materials in solid-state battery, solid polymer electrolyte is usually introduced as an ionic conductive agent, but the electronic insulation of SPE, coupled with random accumulation between particles and uncontrollable polymer coating, makes it difficult to maintain stable interface and continuous electron/ion transport channels (Figure 1a). In this study, NW/rGO composite membrane was prepared by a suction filtration process. rGO helps to improve the conductivity and mechanical stability of cathode materials to construct a stable 3D electron transport framework. Then, PEO solution was dropped on the surface of the NW/rGO composite membrane and penetrated the pores of the 3D framework (Figure 1b). This step can further increase the ionic conductivity of the 3D framework but not sacrifice its original electronic conductivity. Such unique structure simplifies the original complex and chaotic interfaces between particles and changes the point-to-point contact to large-area contact between cathode/SSE, providing continuous channels for rapid electron/ion transport and improved structural stability (Figure 1c). Besides, as a freestanding membrane, its surfaces were also modified to construct two PEO gradient distribution interfaces (Figure 1d). PEO-rich side can provide continuous and strong interface contact with SSE, effectively reduce the cathode/SSE interface impedance. PEO-lack side with the exposed NW/rGO composite thin layer can provide good conductivity and work as the current collector for the integrated freestanding electrode. These gradient interfaces can provide continuous and uniform ionic conductivity, and strengthen the structural integrity for the cathode membrane (Figure 1e). On the contrary, the sharp interfaces in the tape casting homogeneous cathode will cause larger interfacial impedance between SSE and bulk cathode, and lead to interface separation between cathode materials and metal current collector due to the volume expansion during cycling (Figure 1f). It should be emphasized that gradient interfaces only occupy small depth on both surfaces of the cathode membrane, and the main body of the composite cathode is still in a uniformly distributed state of PEO. Under the premise of maintaining the overall integrity of the composite cathode, this modification sufficiently optimizes the interface issues of micro single cathode NW/SSE, the bulk cathode/SSE, and cathode/current collector.

Scanning electron microscope (SEM) images show the morphology of the cathode materials (Figure 2a).  $\text{H}_2\text{V}_3\text{O}_8$  NWs exhibit uniform size of 5–10  $\mu\text{m}$  in length and  $\approx 100$  nm in diameter, and rGO nanosheets are well combined within the randomly oriented NWs. Transmission electron microscope (TEM) characterization was further taken to observe the microscopic structural information. TEM image (Figure 2b) presents the ultrathin geometrical feature of NWs/rGO composite. Large-scale rGO sheets show inseparable contact with NWs, which can reinforce the electrical conductivity and overall firmness for the gradient NW cathode. The high-resolution TEM (HRTEM) image of the NW (Figure 2c) shows the lattice spacing of 0.47 and 0.34 nm, corresponding to the (210) and (011) planes of  $\text{H}_2\text{V}_3\text{O}_8$ , respectively.<sup>[30]</sup> The selected area electron diffraction (SAED) pattern (Figure 2c) reveals that the NW is single crystalline with the corresponding crystal spots of (020) and (011).<sup>[33]</sup>

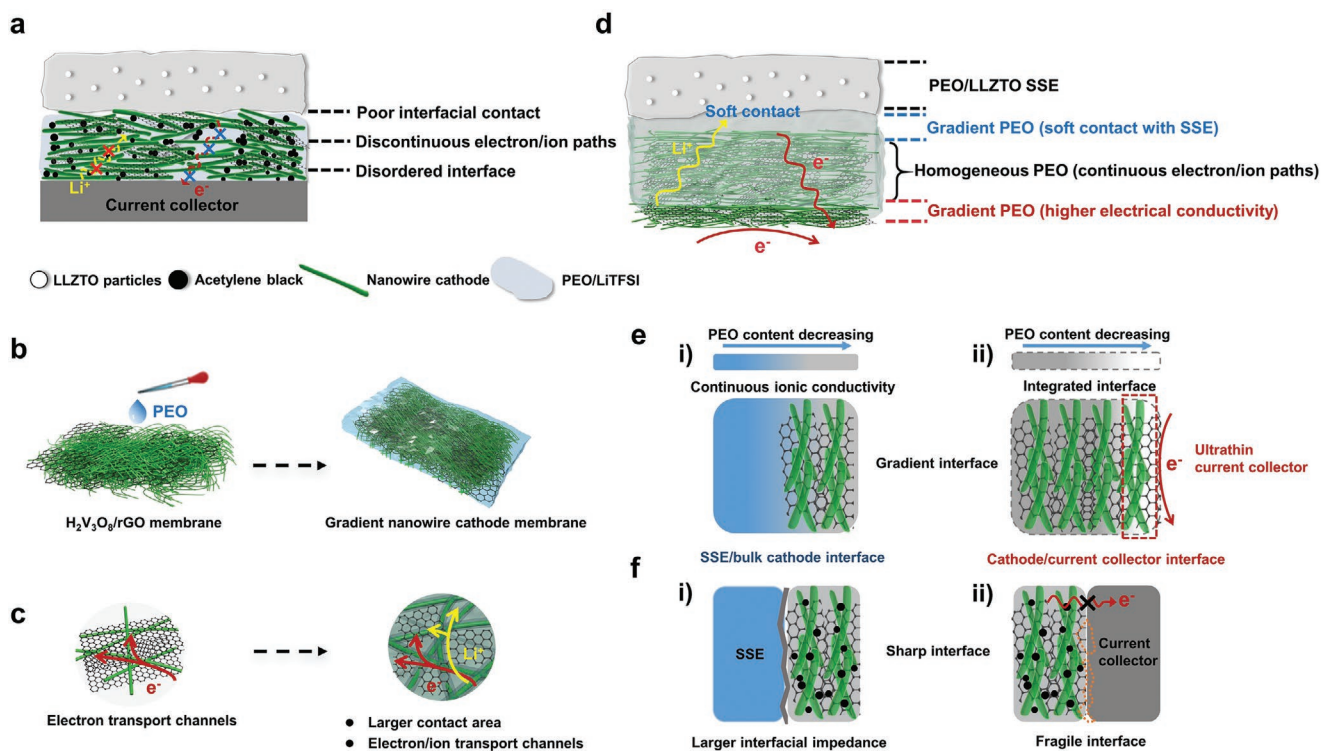


**Figure 1.** Schematics of interface engineering in gradient NW cathode. a) Illustration of interfaces in tape casting homogeneous cathode. b) Preparation process of the gradient NW cathode. c) Internal electron/ion transport characteristics of the gradient NW cathode. d) The distribution and function of the PEO gradient interfaces in the gradient NW cathode, PEO gradient interfaces only occupy a small area, most of PEO is evenly distributed. e) Gradient interfaces in gradient NW cathode, i) SSE/bulk cathode interface, ii) cathode/current collector interface. f) Sharp interfaces in tape casting homogeneous cathode, i) SSE/bulk cathode interface, ii) cathode/current collector interface.

More characterizations were detected to study the structure of cathode materials. X-ray diffraction (XRD) patterns reveal that all the peaks of the cathode materials are in good agreement with the orthorhombic structure of  $\text{H}_2\text{V}_3\text{O}_8$  (PDF#85-2401) (Figure S1, Supporting Information). The only weak peak at  $26^\circ$  can be matched to the diffraction peak of rGO due to its amorphous and low content in the cathode composites.<sup>[34,35]</sup> Thermogravimetry (TG) curve displays the weight loss around  $300^\circ\text{C}$  owing to the structural water (Figure S2, Supporting Information).<sup>[35]</sup> The subsequent 2.5 wt% weight loss of NW/rGO composite at  $300\text{--}600^\circ\text{C}$  is the pyrolysis of rGO. The X-ray photoelectron spectroscopy (XPS) spectra in Figure S3a,b (Supporting Information) give the C 1s spectra of the  $\text{H}_2\text{V}_3\text{O}_8/\text{rGO}$  composites and GO sheets, respectively. The C 1s spectra of  $\text{H}_2\text{V}_3\text{O}_8/\text{rGO}$  exhibit less oxygen-containing functional groups compared to GO, revealing the reduction of GO, which ensures the advanced electrical conductivity between NWs. The V 2p spectra in Figure S3c (Supporting Information) confirm the normal mixed valence states of vanadium.<sup>[36]</sup> These results confirm the stable structure of cathode materials.

The cross-sectional image of gradient NW cathode is presented in Figure 2d, the thickness of gradient NW cathode is  $\approx 34\ \mu\text{m}$ . Although the energy-dispersive spectrometer (EDS) mapping image was not successfully obtained because the bulk polymer was easily decomposed under high energy electron beam, it is still accessible to observe the profiles of NWs throughout the whole membrane. The concentration of

polymer solution was accurately controlled to form the gradient NW cathode, and two different surfaces can be found in Figure 2d. It is obvious that all the gaps in the cathode are filled due to the good concentration of SPE, indicating the firm interfacial contact and mechanical strength. Figure 2e is the enlarged view of the gradient NW cathode. The top side is the polymer-rich surface, the uniform SPE layer provides continuous contact with SSE to decrease the interfacial resistance. The bottom side is the polymer-lack surface to expose a thin layer of NWs/rGO composites with the PEO content gradually decreased, providing the typical electrical conductivity as current collector in the integrated freestanding cathode membrane. This overall structure shows strong integrity, which can provide continuous firm contact between cathode/SSE and avoid the phenomenon that electrode particles separate from the current collector as in tape casting homogeneous cathode.<sup>[5]</sup> Further information about electrical conductivity of gradient NW cathode was given by testing the current–voltage ( $I\text{--}V$ ) characteristics of each surface. The silver paste was carefully brushed on the surface of the membrane as testing electrode and guaranteed not to penetrate the other side. The electrical conductivity can be estimated from Figure 2f, the polymer-lack surface indeed affords higher electronic conductivity, about five orders of magnitude than the polymer-rich side. This result suggests that improved electronic conduction can be realized for the gradient cathode because of the modified polymer-lack surface.

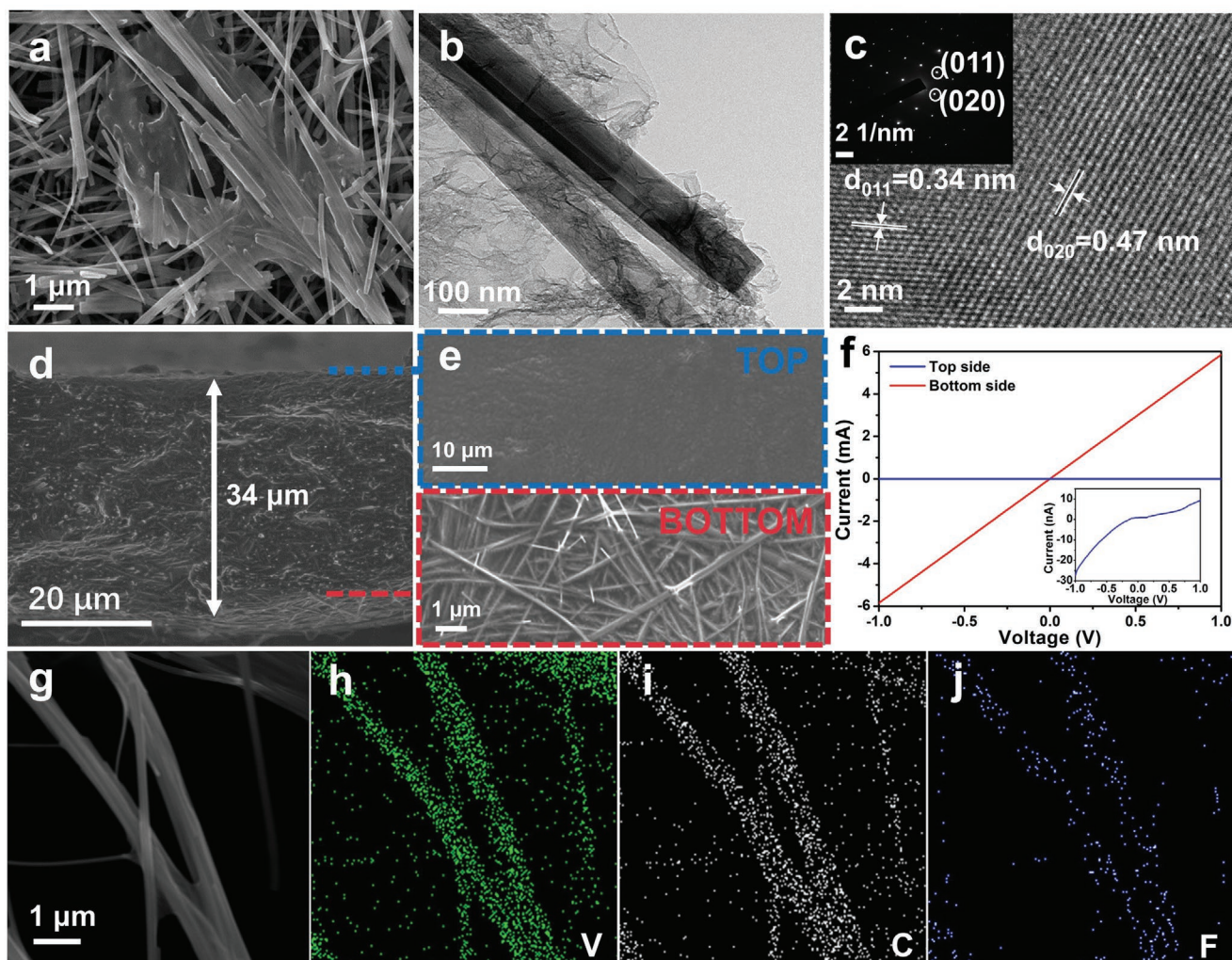


**Figure 2.** Electron microscopy and transport characterizations of gradient NW cathode. a) SEM image of the  $\text{H}_2\text{V}_3\text{O}_8$  NWs/rGO composite. b) TEM image of the  $\text{H}_2\text{V}_3\text{O}_8$  NWs/rGO composite. c) HRTEM image of the NW showing the single-crystalline lattice of  $\text{H}_2\text{V}_3\text{O}_8$ . Inset is the corresponding SAED image. d) Cross-sectional SEM image of the gradient NW cathode. e) SEM images of two surfaces of gradient NW cathode. f) Transport properties of different gradient NW cathode surfaces, the inset is the transport properties of bottom side. g) Individual polymer-coated NWs in gradient NW cathode and EDS mapping of h–j) V, C, F elements.

To sort out the state of polymer wetting, a few polymer-coated NWs inside the membrane from the artificially damaged part were detected (Figure 2g), where stable polymer-coated structure can be clearly observed. Every single NW is uniformly coated by SPE, which can afford fast lithium-ion transport pathways. In addition, the flexibility of NWs and SPE can reinforce the interfacial contact to buffer the volume change during cycling. Figure 2h–j displays the distribution of V, C, F elements, respectively. F element displays the distribution of V, C, F elements, respectively. F element comes from lithium salt LiTFSI in the SPE, and it is obvious that the uniform interfacial contact between single NW cathode and SPE is realized. The lithium salt in the SPE is uniformly enriched on the NW surface, which can provide continuous lithium-ion supply during cycling. Therefore, the intricate interface issues of inside single NW cathode/SSE, the bulk cathode/SSE and cathode/current collector are simplified and optimized by a facile solvent evaporation process. This integrated gradient NW cathode membrane can be regarded as a steady continuous electron/ion transport framework.

The SSE was fabricated by mixing a suitable amount of  $\text{Li}_{6.4}\text{La}_3\text{Zr}_{1.4}\text{Ta}_{0.6}\text{O}_{12}$  (LLZTO) particles with PEO/LiTFSI solution.<sup>[37]</sup> Electrochemical impedance spectroscopy (EIS) test was conducted at the temperature from 20 to 80 °C (Figure S4, Supporting Information). The calculated ionic conductivity of SSE is  $1.03 \times 10^{-4} \text{ S cm}^{-1}$  at room temperature. The electrochemical stability of SSE was tested by linear sweep voltammetry (LSV; Figure S5, Supporting Information). The electrochemical window of the SSE is 5 V, offering a potential possibility for the application of high-voltage cathode materials due to the addition of high oxidative stability of LLZTO and Lewis acid-base interaction between LLZTO and TFSI<sup>-</sup> anions.<sup>[38]</sup> The lithium compatibility test of SSE was performed with a current of 0.2 mA at 50 °C (2 h for a cycle) and the result is shown in Figure S6 (Supporting Information). The polarization potential of the symmetric battery is about 50 mV. No short-circuit is observed and the polarization potential is steady after cycling for 500 h. TG curve of the solid electrolyte, executed in the Ar atmosphere

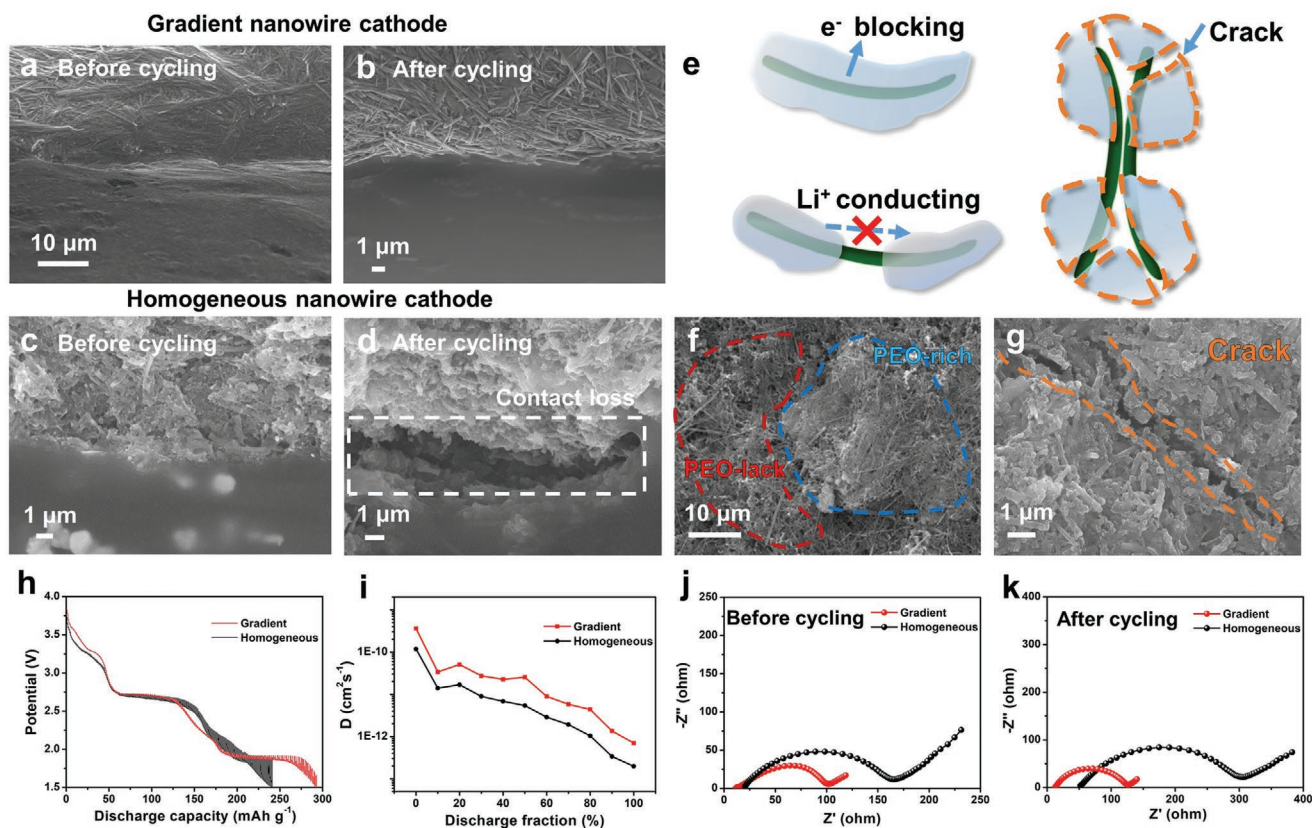


**Figure 3.** Cross-sectional SEM images of cathode/SSE interfaces before and after cycling: a,b) Gradient NW cathode, c,d) homogeneous NW cathode. e) Schematics of the possible issues in tape casting homogeneous cathode, e.g.,  $e^-$  blocking,  $\text{Li}^+$  blocking, and crack after cycling. f) SEM image of homogeneous cathode, PEO-rich and PEO-lack area are circled to demonstrate the  $e^-$  blocking and  $\text{Li}^+$  blocking, respectively. g) Cross-sectional SEM image of the homogeneous cathode after cycling. h) GITT curves and i) the relationship of the diffusion coefficients versus discharge fraction. Nyquist plots of SSLBs with gradient NW cathode and homogeneous NW cathodes: j) before cycling and k) after 100 cycles.

from 25 to 600  $^{\circ}\text{C}$  (Figure S7, Supporting Information), illustrates that weight loss occurs in the pyrolysis process of the solid electrolyte at 300  $^{\circ}\text{C}$ . The results show solid electrolyte possesses excellent thermal stability, and no obvious weight loss occurs in the temperature ranging from 25 to 150  $^{\circ}\text{C}$ , implying the composite SSE can effectively work under high temperature.

For a better understanding of the cathode/SSE interface, SEM images of the cathode/electrolyte interface are presented in Figure 3a–d. The continuous cross-sectional morphology in the gradient NW cathode suggests closer interfacial contacts (Figure 3a). After cycling, the gradient NW cathode still remains the continuous and firm interfacial contact with SSE (Figure 3b), and no degradation in the bulk cathode can be seen, indicating the durable gradient structure. It is obvious that the contact between the homogeneous NW cathode and SSE is rigid (Figure 3c). Moreover, in the homogeneous NW cathode, the sharp SSE/bulk cathode interface and point-to-point contact of NWs are not accessible to fast  $\text{Li}^+$  transport. After cycling, there is an enormous crack between the homogeneous NW cathode/SSE interface, this giant contact loss will directly ruin the regular operation of batteries (Figure 3d). Figure 3e is the schematic diagram of possible issues in tape casting homogeneous cathode. Limited by the preparation process, the coating process is just simple stacking of the

composite materials. Active materials, conductive additives, and solid polymer electrolyte are mixed disorderly in the cathode slurry, thus PEO polymer electrolyte cannot achieve uniform coating on the cathode materials as expected, which is difficult to construct continuous electron/ion transport channels for the cathode in SSLB system. Excessive coating of PEO will hinder the conduction of electrons on the surface of cathode materials. Incomplete PEO coating will block the transmission of lithium ions. In addition, disordered stacking is difficult to maintain a close connection between cathode materials, so that the volume expansion will cause cracks during cycling. Figure 3f shows the PEO-rich area and PEO-lack area in the same cathode surface, indicating the inadequate PEO coating. Figure 3g shows the obvious crack in homogeneous cathode after cycling. This poor interface compatibility will greatly increase the interface impedance and aggravate the failure of the solid–solid contact.

To investigate the lithium-ion diffusion efficiency for gradient NW cathode, galvanostatic intermittent titration technique (GITT) was employed to study the diffusion kinetics of  $\text{Li}^+$ . The overall discharge curves are presented in Figure 3h. After the introduction of the polymer coating, the polarization is significantly reduced throughout the range and a high discharge capacity of 290  $\text{mAh g}^{-1}$  is achieved. Figure 3i shows the lithium-ion diffusion coefficient ( $D_s$ ) of

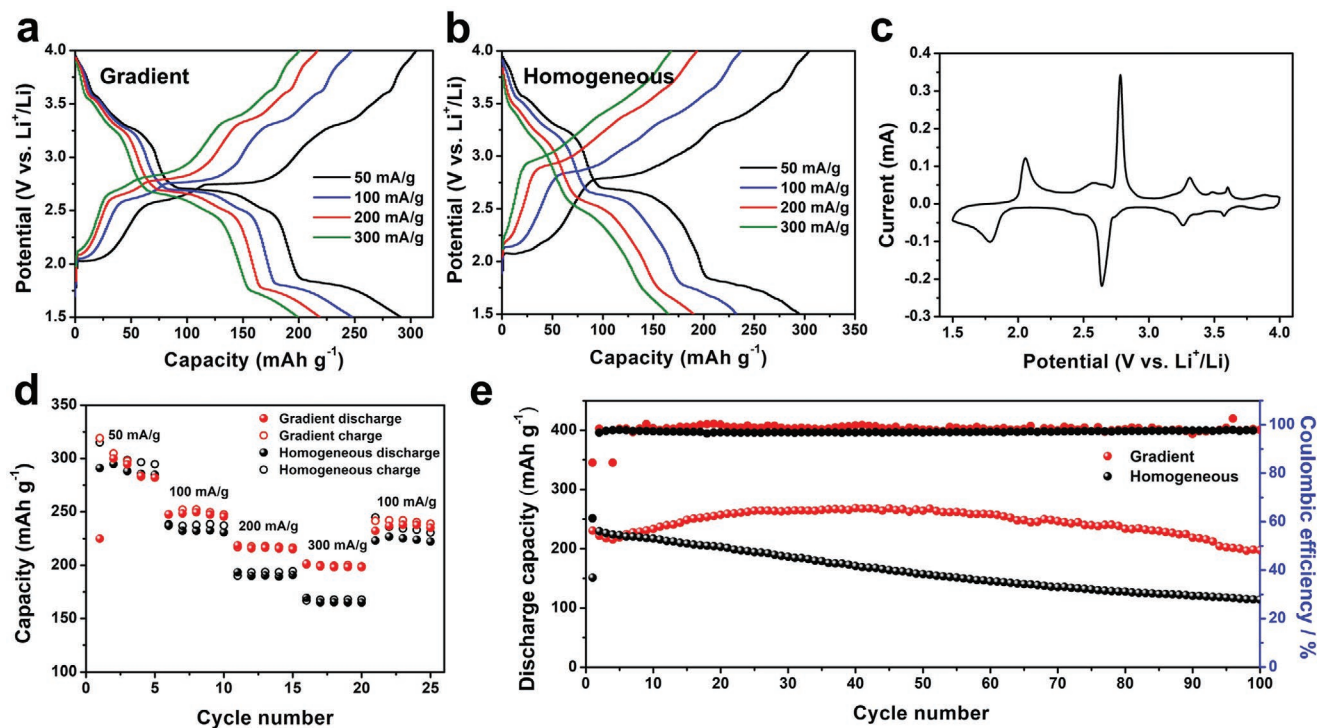


**Figure 4.** Electrochemical performance of gradient NW cathode for SSLBs. The charge/discharge profiles of a) gradient NW cathode and b) homogeneous NW cathode at the current density ranging from 50 to 300 mA g<sup>-1</sup> based on SSE. c) CV curve of homogeneous NW cathode with liquid electrolyte at a scanning rate of 0.1 mV s<sup>-1</sup>. d) Rate capability at the current density ranging from 50 to 300 mA g<sup>-1</sup> based on SSE. e) Cycling performance of gradient NW cathode at 100 mA g<sup>-1</sup> based on SSE at room temperature.

homogeneous NW cathode and gradient NW cathode in different discharge fraction, respectively.<sup>[11,39]</sup> The gradient NW cathode illustrates significantly increased  $D_s$  in the range of 0.1–10 × 10<sup>-11</sup> cm<sup>2</sup> s<sup>-1</sup>, which is about three times higher than the homogeneous NW cathode. The improved  $D_s$  of gradient NW cathode demonstrates faster lithium-ion diffusion because of the consequent electron/ion transport pathways and much more sustained interfacial contact in the NW cathode. These results imply that the gradient NW cathode gives a powerful contribution to fast lithium-ion diffusion, resulting in improved electrochemical performance. As for the interfacial resistance, EIS test was conducted at the voltage of around 3.2 V for SSLBs before and after cycling (Figure 3j,k). Before cycling, the charge transfer resistance of gradient NW cathode is around 125 Ω, and it is a little larger at about 160 Ω for homogeneous cathode. After 100 cycles, the resistance increases for both cathodes, while the resistance of the gradient NW cathode still keeps much lower than the homogeneous NW cathode. It is demonstrated that the gradient NW cathode effectively ameliorated interface issues of the bulk cathode/SSE and the inside NW cathode materials, providing continuous and uniform electron/ion transport channels and enhanced structural integrity.

Charge–discharge curves of SSLBs with gradient NW cathode and homogeneous NW cathode are shown in Figure 4a,b, respectively. As shown in Figure 4a, SSLB with gradient NW cathode presents smooth charge–discharge curves at different current densities. The charge and discharge platforms are consistent with the redox peaks in cycle voltammetry (CV) curves

of lithium battery with liquid electrolyte (Figure 4c).<sup>[35]</sup> In Figure 4b, as the current density increasing, SSLB with homogeneous NW cathode shows extreme polarization because of the larger resistance caused by uneven PEO coating and poor contact in sharp interfaces during cycling. In addition, poor interface compatibility also results in capacity decay under elevated current densities. This result indicates improved properties of lithium-ion insertion/extraction on account of the reliable interface stability and rapid electron/ion transport channels in the gradient NW electrode. Rate performances under current density from 50 to 300 mA g<sup>-1</sup> at room temperature are presented in Figure 4d. The cell with homogeneous NW cathode has a specific capacity of around 300 mAh g<sup>-1</sup> at the current density of 50 mA g<sup>-1</sup> as same as the gradient NW cathode. However, with the current density increasing, the capacity drops sharply and only remains 140 mAh g<sup>-1</sup> at the current density of 300 mA g<sup>-1</sup>. The chaotic electron/ion transport channels in homogeneous NW cathode make it difficult to adapt to sudden changes of current density, the sluggish electron/ion transport will result in poor stability and rapid capacity decay. On the contrary, the gradient NW cathode exhibits more excellent rate performance. The specific capacity still maintains more than 200 mAh g<sup>-1</sup> when the current density gradually increases to 300 mA g<sup>-1</sup>. When the rate is back to 100 mA g<sup>-1</sup>, the specific capacity returned to 240 mAh g<sup>-1</sup>, which is only a little lower than the capacity of cathode in the liquid electrolyte (Figure S8, Supporting Information) due to the inferior ionic conductivity of SSE versus organic liquid electrolyte. This superior rate performance relies on the enhanced cathode/electrolyte interface

contact and continuous electron/ion transport in the SSLBs. Figure 4e indicates the long cycling performance under the current density of 100 mA g<sup>-1</sup> at room temperature. The initial discharge capacities of both gradient NW cathode and homogeneous NW cathode delivered capacity around 230 mAh g<sup>-1</sup>. The capacity of SSLB with freestanding gradient NW cathode decreases at the beginning because it demands more time to optimize due to the inferior electronic conductivity than the metal current collector. Then the capacity of gradient NW cathode cell increases a little and gradually becomes relatively stable in the following cycles and finally remains the capacity of 200 mAh g<sup>-1</sup> after 100 cycles. The enhanced capacity retention and cycling stability of gradient NW cathode are contributed to the fast electron/ion transport channels and sustained interfacial contact by the interface engineering. However, the capacity of the homogeneous NW cathode cell shows a continuous decline caused by the disordered connection and poor adhesive characteristic of the cathode/SSE interface. The SSLBs with gradient NW cathode show superior electrochemical performance in the interface engineering field (Table S1, Supporting Information). This modification is suitable for the most of 1D electrode materials, which can go through a better match between high-performance cathode materials and SSE to fabricate advanced SSLBs with high energy density and cycling stability.

### 3. Conclusion

In conclusion, interface engineering on a gradient NW electrode by a facile solvent evaporation process is demonstrated. In this gradient composite system, interfaces of cathode/SSE, cathode/current collector, and inner structures of cathode are modulated by accurately controlling the concentration of polymer solution. The obtained gradient structure with two different factional surfaces delivers both the smooth contact between cathode/SSE interface and fast electron transport as current collector, respectively. Furthermore, the composite architecture with large-area interface contact between inner cathode particles and steady structural strength can significantly increase the electron/ion transport and buffer volume variation during cycling. Effective interface engineering endows the SSLBs with reduced interfacial resistance, high capacity, and enhanced cycling stability. This novel gradient interface engineering strategy can be further extended for other nanostructured electrode materials, which is of great potential for the development of next-generation high-performance SSLBs.

### 4. Experimental Section

*Preparation of the H<sub>2</sub>V<sub>3</sub>O<sub>8</sub> NWs Membrane:* The H<sub>2</sub>V<sub>3</sub>O<sub>8</sub> NWs were synthesized by hydrothermal synthesis method according to the literature. First, 10 mL hydrogen peroxide solution (H<sub>2</sub>O<sub>2</sub>) was added into 0.237 g of vanadium pentoxide (V<sub>2</sub>O<sub>5</sub>) and the mixture was stirred vigorously. After that 50 mL deionized (DI) water and 0.04 g poly(ethylene glycol) (PEG-4000) were added to vanadium sol, respectively. Meanwhile, graphene oxide (GO) solution (obtained by Hummers method) was dispersed and then transferred to the vanadium sol solution, and the obtained solution was stirred continuously for 1 day. Finally, the solution was transferred to a 100 mL autoclave and kept in the oven at 180 °C for

2 days. The products were washed three times alternately with water and ethanol, and then dried at 70 °C in the air for 12 h to obtain the H<sub>2</sub>V<sub>3</sub>O<sub>8</sub> NWs/rGO composite. Afterward, 25 mg H<sub>2</sub>V<sub>3</sub>O<sub>8</sub> NWs/rGO composite were dispersed in water and sonicated for 2.5 h, then the dispersion was filtered and the products were dried at 70 °C to obtain H<sub>2</sub>V<sub>3</sub>O<sub>8</sub> NWs/rGO composite membrane.

*Preparation of the SSE Membrane:* First, PEO (M<sub>v</sub> = 10<sup>6</sup> g mol<sup>-1</sup>, Sigma Aldrich), LiTFSI (Aladdin), and LLZTO (HEFEI KEJING) were successively added into 20 mL anhydrous acetonitrile. Among these, the molar ratio of EO and Li<sup>+</sup> was 8:1 and LLZTO accounted for 15 wt% of the overall solid particles. Then the mixture was blended by magnetic stirring for 24 h to obtain the homogeneous electrolyte slurry. The solid electrolyte membrane was obtained by blading the slurry on a polytetrafluoroethylene plate and dried in an argon-filled glove box for 12 h, and then the solid electrolyte membrane was further dried in the vacuum oven at 60 °C for 24 h. Finally, the electrolyte membrane with thickness of ≈100 μm was produced. All the preparation processes should be carried out in an Ar-filled glovebox with H<sub>2</sub>O and O<sub>2</sub> contents below 0.1 ppm.

*Preparation of the Gradient NW Cathode:* The same method as the preparation of the solid electrolyte membrane was used to prepare the electrolyte solution with the molar ratio of 10:1 (EO:Li<sup>+</sup>). Homogeneous electrolyte slurry was then cast on the prepared H<sub>2</sub>V<sub>3</sub>O<sub>8</sub> NWs/rGO composite membrane directly to achieve the composite gradient NW cathode membrane. The composite cathode material was initially dried at 60 °C in the vacuum oven for 24 h. The H<sub>2</sub>V<sub>3</sub>O<sub>8</sub> active material loading was ≈1.5 mg cm<sup>-2</sup> for the gradient NW cathode.

*Materials Characterizations:* XRD patterns were recorded using a D8 discover X-ray diffractometer with Cu Kα radiation. The surface area and pore-size distribution were calculated from N<sub>2</sub> adsorption isotherms measured by using a Tristar-3020 instrument. The thermal stability was executed by thermogravimetric analysis (TGA) using a NETZSCH STA 449F5 instrument over the temperature range between 25 and 600 °C under Ar flux at a heating rate of 10 °C min<sup>-1</sup>. XPS tests were further carried out by the VG Multi Lab 2000. The morphology of H<sub>2</sub>V<sub>3</sub>O<sub>8</sub> NWs membrane and H<sub>2</sub>V<sub>3</sub>O<sub>8</sub>/PEO composite cathode was represented by a field-emission scanning electron microscopy (JEOL-7100F) after gold spraying. EDS was collected by an Oxford IE250 system. TEM images were collected using JEM-1400plus. TEM and HRTEM images were recorded by using a JEM-2100F microscope.

*Electrochemical Measurements:* Electrochemical impedance spectroscopy was tested by assembling blocking stainless steel|SSE|stainless steel cell from 0.1 Hz to 1 MHz with an amplitude of 10 mV via Autolab PGSTAT302N. The electrochemical stability window was analyzed by LSV on a lithium|SSE|stainless steel cell from open-circuit voltage to 6.5 V at a scan rate of 0.5 mV s<sup>-1</sup>. The cycling stability of lithium|SSE|lithium, and SSLB was conducted using a multichannel battery testing system (LAND CT2001A). Homogeneous cathode materials were composed of 70 wt% H<sub>2</sub>V<sub>3</sub>O<sub>8</sub> NWs/rGO composite materials, 15 wt% acetylene black conductive additive, and 15 wt% PEO/LiTFSI, molar ratio of EO and Li<sup>+</sup> was 10:1, and then the mixing slurry was coated on the Al foil current collector. The H<sub>2</sub>V<sub>3</sub>O<sub>8</sub> active material loading was ≈1.5 mg cm<sup>-2</sup> for homogeneous cathode. 2016 coin cells were assembled with cathode, SSE, and lithium metal anodes via ordinal stacking. Little ionic liquid (5 μL) was added only between lithium metal anode and SSE, and there was no ionic liquid added at the interface between cathode and SSE. The ionic liquid at anode/SSE interface was to achieve good interfacial wetting and would be helpful for the stable SEI formation.<sup>[40]</sup> The ionic liquid (EMIM<sub>0.83</sub>Li<sub>0.17</sub>)TFSI was prepared by mixing LiTFSI and (EMIM)TFSI through magnetic stirring.<sup>[41]</sup> All the electrochemical properties of SSLBs were tested at room temperature, lithium compatibility test of SSE was conducted at 50 °C.

*Calculation for Ionic Conductivity:* The bulk resistance (R<sub>b</sub>) of SSEs was obtained from the EIS spectrum. The ionic conductivity was calculated from Equation (1)

$$\sigma = \frac{L}{R_b S} \quad (1)$$

where  $R_b$  is the bulk resistance,  $L$  is the thickness, and  $S$  is the area of the SSEs, respectively.

*Calculation for the Apparent Diffusion Coefficients:* Calculation for the apparent diffusion coefficients of  $\text{Li}^+$  ions through GITT results: The  $D^{\text{GITT}}$  could be obtained through the potential variation to an intermittent invariable current pulse. The detailed calculation was carried out from Equation (2)

$$D^{\text{GITT}} = \frac{4}{\pi\tau} \left( \frac{n_m V_m}{S} \right)^2 \left( \frac{\Delta E_s}{\Delta E_t} \right)^2 \quad (2)$$

where  $\tau$  represents the time for an individual constant current pulse and  $n_m$ ,  $V_m$ , and  $S$  indicate the molar number, molar volumes, and electrode-electrolyte contact area, respectively.  $\Delta E_t$  is the integral difference of cell voltage for charging or discharging, and the voltage variation during the individual open-circuit period can be denoted as  $\Delta E_s$ .<sup>[39]</sup> The cells were charged for 10 min at constant current of 10 mA  $\text{g}^{-1}$  and rested for 30 min until the voltage reached 4.0 V and discharged for the same progress until the voltage reached 1.5 V.

## Supporting Information

Supporting Information is available from the Wiley Online Library or from the author.

## Acknowledgements

Y.C. and J.S. contributed equally to this work. This work was supported by the National Key Research and Development Program of China (2020YFA0715000), the National Natural Science Foundation of China (51802239), the Foshan Xianhu Laboratory of the Advanced Energy Science and Technology Guangdong Laboratory (XHT2020-005, XHT2020-003), the Natural Science Foundation of Hubei Province (2019CFA001), the National Key Research and Development Program of China (2019YFA0704902), the Fundamental Research Funds for the Central Universities (2020111011GX, 2020IVB057, 2019IVB054, and 2019111062JL), and National Innovation and Entrepreneurship Training Program for College Students (202010497080).

## Conflict of Interest

The authors declare no conflict of interest.

## Data Availability Statement

Research data are not shared.

## Keywords

gradient, interface engineering, nanowires, solid-state batteries

Received: January 4, 2021

Published online:

[1] S. Xin, Y. You, S. Wang, H.-C. Gao, Y.-X. Yin, Y.-G. Guo, *ACS Energy Lett.* **2017**, *2*, 1385.

[2] L. Fan, S. Wei, S. Li, Q. Li, Y. Lu, *Adv. Energy Mater.* **2018**, *8*, 1702657.

- [3] D. Zhou, R. Liu, Y.-B. He, F. Li, M. Liu, B. Li, Q.-H. Yang, Q. Cai, F. Kang, *Adv. Energy Mater.* **2016**, *6*, 1502214.
- [4] L. Xu, S. Tang, Y. Cheng, K. Wang, J. Liang, C. Liu, Y.-C. Cao, F. Wei, L. Mai, *Joule* **2018**, *2*, 1991.
- [5] Y. Xiao, Y. Wang, S.-H. Bo, J. C. Kim, L. J. Miara, G. Ceder, *Nat. Rev. Mater.* **2020**, *5*, 105.
- [6] S. P. Culver, R. Koerver, W. G. Zeier, J. Janek, *Adv. Energy Mater.* **2019**, *9*, 1900626.
- [7] Z. Gao, H. Sun, L. Fu, F. Ye, Y. Zhang, W. Luo, Y. Huang, *Adv. Mater.* **2018**, *30*, 1705702.
- [8] R. Chen, Q. Li, X. Yu, L. Chen, H. Li, *Chem. Rev.* **2019**, *120*, 6820.
- [9] L. Mai, M. Yan, Y. Zhao, *Nature* **2017**, *546*, 469.
- [10] J. Lau, R. H. DeBlock, D. M. Butts, D. S. Ashby, C. S. Choi, B. S. Dunn, *Adv. Energy Mater.* **2018**, *8*, 1800933.
- [11] J.-Y. Liang, X.-X. Zeng, X.-D. Zhang, P.-F. Wang, J.-Y. Ma, Y.-X. Yin, X.-W. Wu, Y.-G. Guo, L.-J. Wan, *J. Am. Chem. Soc.* **2018**, *140*, 6767.
- [12] F. Han, Y. Zhu, X. He, Y. Mo, C. Wang, *Adv. Energy Mater.* **2016**, *6*, 1501590.
- [13] M. Du, K. Liao, Q. Lu, Z. Shao, *Energy Environ. Sci.* **2019**, *12*, 1780.
- [14] L.-P. Wang, X.-D. Zhang, T.-S. Wang, Y.-X. Yin, J.-L. Shi, C.-R. Wang, Y.-G. Guo, *Adv. Energy Mater.* **2018**, *8*, 1801528.
- [15] H. Duan, M. Fan, W.-P. Chen, J.-Y. Li, P.-F. Wang, W.-P. Wang, J.-L. Shi, Y.-X. Yin, L.-J. Wan, Y.-G. Guo, *Adv. Mater.* **2019**, *31*, 1807789.
- [16] T. Shi, Q. Tu, Y. Tian, Y. Xiao, L. J. Miara, O. Kononova, G. Ceder, *Adv. Energy Mater.* **2020**, *10*, 1902881.
- [17] L. Yang, Z. Wang, Y. Feng, R. Tan, Y. Zuo, R. Gao, Y. Zhao, L. Han, Z. Wang, F. Pan, *Adv. Energy Mater.* **2017**, *7*, 1701437.
- [18] X. Han, Y. Gong, K. K. Fu, X. He, G. T. Hitz, J. Dai, A. Pearse, B. Liu, H. Wang, G. Rubloff, Y. Mo, V. Thangadurai, E. D. Wachsman, L. Hu, *Nat. Mater.* **2017**, *16*, 572.
- [19] D. Cao, Y. Zhang, A. M. Nolan, X. Sun, C. Liu, J. Sheng, Y. Mo, Y. Wang, H. Zhu, *Nano Lett.* **2019**, *20*, 1483.
- [20] X. Chen, W. He, L.-X. Ding, S. Wang, H. Wang, *Energy Environ. Sci.* **2019**, *12*, 938.
- [21] D. Wang, Q. Sun, J. Luo, J. Liang, Y. Sun, R. Li, K. Adair, L. Zhang, R. Yang, S. Lu, H. Huang, X. Sun, *ACS Appl. Mater. Interfaces* **2019**, *11*, 4954.
- [22] R. Koerver, I. Aygün, T. Leichtweiß, C. Dietrich, W. Zhang, J. O. Binder, P. Hartmann, W. G. Zeier, J. Janek, *Chem. Mater.* **2017**, *29*, 5574.
- [23] J. Zhang, N. Zhao, M. Zhang, Y. Li, P. K. Chu, X. Guo, Z. Di, X. Wang, H. Li, *Nano Energy* **2016**, *28*, 447.
- [24] J. Bae, Y. Li, J. Zhang, X. Zhou, F. Zhao, Y. Shi, J. B. Goodenough, G. Yu, *Angew. Chem., Int. Ed.* **2018**, *57*, 2096.
- [25] L. Yu, S. Guo, Y. Lu, Y. Li, X. Lan, D. Wu, R. Li, S. Wu, X. Hu, *Adv. Energy Mater.* **2019**, *9*, 1900257.
- [26] K. Fu, Y. Gong, J. Dai, A. Gong, X. Han, Y. Yao, C. Wang, Y. Wang, Y. Chen, C. Yan, Y. Li, E. D. Wachsman, L. Hu, *Proc. Natl. Acad. Sci. U. S. A.* **2016**, *113*, 7094.
- [27] L. Mai, X. Tian, X. Xu, L. Chang, L. Xu, *Chem. Rev.* **2014**, *114*, 11828.
- [28] Z. Wan, D. Lei, W. Yang, C. Liu, K. Shi, X. Hao, L. Shen, W. Lv, B. Li, Q.-H. Yang, F. Kang, Y.-B. He, *Adv. Funct. Mater.* **2019**, *29*, 1805301.
- [29] D. Zhou, Y.-B. He, R. Liu, M. Liu, H. Du, B. Li, Q. Cai, Q.-H. Yang, F. Kang, *Adv. Energy Mater.* **2015**, *5*, 1500353.
- [30] Q. Pang, C. Sun, Y. Yu, K. Zhao, Z. Zhang, P. M. Voyles, G. Chen, Y. Wei, X. Wang, *Adv. Energy Mater.* **2018**, *8*, 1800144.
- [31] B. Liu, K. Fu, Y. Gong, C. Yang, Y. Yao, Y. Wang, C. Wang, Y. Kuang, G. Pastel, H. Xie, E. D. Wachsman, L. Hu, *Nano Lett.* **2017**, *17*, 4917.
- [32] Y. Zhang, J. Lai, Y. Gong, Y. Hu, J. Liu, C. Sun, Z. L. Wang, *ACS Appl. Mater. Interfaces* **2016**, *8*, 34309.
- [33] P. He, Y. Quan, X. Xu, M. Yan, W. Yang, Q. An, L. He, L. Mai, *Small* **2017**, *13*, 1702551.
- [34] C. Zhang, H. Song, C. Zhang, C. Liu, Y. Liu, G. Cao, *J. Phys. Chem. C* **2015**, *119*, 11391.
- [35] Q. An, J. Sheng, X. Xu, Q. Wei, Y. Zhu, C. Han, C. Niu, L. Mai, *New J. Chem.* **2014**, *38*, 2075.



- [36] Y. Dai, Q. Li, S. Tan, Q. Wei, Y. Pan, X. Tian, K. Zhao, X. Xu, Q. An, L. Mai, Q. Zhang, *Nano Energy* **2017**, *40*, 73.
- [37] L. Chen, Y. Li, S.-P. Li, L.-Z. Fan, C.-W. Nan, J. B. Goodenough, *Nano Energy* **2018**, *46*, 176.
- [38] W. Zha, F. Chen, D. Yang, Q. Shen, L. Zhang, *J. Power Sources* **2018**, *397*, 87.
- [39] M. Qin, W. Ren, J. Meng, X. Wang, X. Yao, Y. Ke, Q. Li, L. Mai, *ACS Sustainable Chem. Eng.* **2019**, *7*, 11564.
- [40] M. Watanabe, M. L. Thomas, S. Zhang, K. Ueno, T. Yasuda, K. Dokko, *Chem. Rev.* **2017**, *117*, 7190.
- [41] Y. Xia, N. Xu, L. Du, Y. Cheng, S. Lei, S. Li, X. Liao, W. Shi, L. Xu, L. Mai, *ACS Appl. Mater. Interfaces* **2020**, *12*, 22930.